International Journal of
Molecular Sciences

MDPI

Article

Theoretical Analysis for Wireless Magnetothermal Deep Brain Stimulation Using Commercial Nanoparticles

Tuan-Anh Le, Minh Phu Bui and Jungwon Yoon *

Gwangju Institute of Science and Technology, School of Integrated Technology, 123 Cheomdan-gwagiro, Buk-gu, Gwangju 61005, Korea; tuananhle@gist.ac.kr (T.-A.L.); buiminhphu@gist.ac.kr (M.P.B.)
* Correspondence: jyoon@gist.ac.kr; Tel.: +82-62-715-5332

Received: 6 May 2019; Accepted: 10 June 2019; Published: 12 June 2019

Abstract: A wireless magnetothermal stimulation (WMS) is suggested as a fast, tetherless, and implanted device-free stimulation method using low-radio frequency (100 kHz to 1 MHz) alternating magnetic fields (AMF). As magnetic nanoparticles (MNPs) can transduce alternating magnetic fields into heat, they are targeted to a region of the brain expressing the temperature-sensitive ion channel (TRPV1). The local temperature of the targeted area is increased up to 44 °C to open the TRPV1 channels and cause an influx of Ca^{2+} sensitive promoter, which can activate individual neurons inside the brain. The WMS has initially succeeded in showing the potential of thermomagnetics for the remote control of neural cell activity with MNPs that are internally targeted to the brain. In this paper, by using the steady-state temperature rise defined by Fourier's law, the bio-heat equation, and COMSOL Multiphysics software, we investigate most of the basic parameters such as the specific loss power (SLP) of MNPs, the injection volume of magnetic fluid, stimulation and cooling times, and cytotoxic effects at high temperatures (43–44 °C) to provide a realizable design guideline for WMS.

Keywords: wireless magnetothermal stimulation; deep brain stimulation; magnetic particles

1. Introduction

Stimulation of the deep brain has shown outstanding performance for people with neurological problems such as Parkinson's disease, essential tremor and so on [1]. Currently, the simulation method has been deployed using permanently implanted electrodes [2] and chemicals [3], acoustic [4], electromagnetic [5], or optical [6] signals. However, these methods often show un-specific stimulation or poor penetration of visible light into deep tissues, or sometimes require implanted devices for deep brain stimulation [3,6]. To overcome some of these limitations, a few groups have come up with new, competing technologies that exploit the properties of magnetic nanoparticles (MNPs). The current MNPs have shown many pre-eminent features such as a uniform size, consistent thermal, magnetic properties and coating technology [7] and are suitable for most biomedical applications such as drug delivery, imaging, and cancer hyperthermia [8,9]. MNPs (with a size range of 10–50 nm) are small enough or can be surface-modified with transferrin antibodies [10] to traverse the blood–brain barrier and can transduce alternating magnetic fields (AMF) into heat. Although MNP heating has been studied as a cell-kill therapy in magnetic hyperthermia for over 50 years [11], applying the hyperthermia method to remotely influence cellular activities has only been researched in recent years. The new method for brain stimulation using magnetic hyperthermia is called the wireless magnetothermal stimulation (WMS) method [12,13]. A method with quite a similar name, 'transcranial magnetic stimulation' (TMS), also exists [14]. However, it is different from WMS as it uses electromagnetic induction to stimulate the brain [14].

The WMS method has been suggested to provide a fast, tetherless, and implanted device-free method utilizing alternating magnetic fields (AMF) with ranges of 100 kHz to 1 MHz and magnetic nanoparticles (MNPs) with size range of 10–50 nm to dissipate hysteretic power loss [13]. Due to their quality of transducing alternating magnetic fields into heat, as a principle, the MNPs are targeted at neural cells expressing the temperature-sensitive ion channel (TRPV1). The local temperature of the targeted area is then increased up to 44 °C to open the TRPV1 channels and produce an influx of Ca^{2+}-sensitive promoter [15,16] that can activate individual neurons inside the brain. In 2010, Huang et al., first demonstrated in [17] that the magnetic field heating of superparamagnetic nanoparticles (SNPs) could stimulate action potentials in primary hippocampal neurons. Two years later, Stanley et al., described regulated insulin production in mice with a similar method using a radio wave at 465 kHz [18]. In 2015, Chen et al. demonstrated the ability to remotely excite in vivo neuronal circuits using thermomagnetics with AMF at a frequency of 500 kHz, and a magnetic field strength of 15 kA/m [13]. In 2017, Rahul et al., used WMS for motor behavior in awake, freely moving mice [19]. Initial explorations of WMS have successfully shown the potential of thermomagnetics for the remote control of neural cell activity with MNPs that are internally targeted to the brain. However, there are no studies that have comprehensively investigated the effects of the specific loss power (SLP) of MNPs, stimulation volume (occupied by the magnetic nanoparticles), stimulation and cooling times, and cytotoxic effects at high temperatures (43–44 °C) to suggest the feasible conditions for using WMS.

To provide design guidelines for WMS experiments, this study presents a theoretical analysis of WMS using the steady-state temperature rise defined by Fourier's law, the bio-heat equation and COMSOL Multiphysics software to investigate the basic parameters. This paper is organized as follows: in Section 2, the simulation results and discussions are presented. In Section 3, the materials and methods are introduced. Section 4 consists of the conclusion and future works.

2. Results and Discussion

2.1. Preliminary Determination of Minimum Limits for WMS without Blood Flow and Cerebrospinal Fluid (CSF)

Figure 1 shows the steady-state temperature with different SLPs, concentrations (ς_{MNPs}) and injection volumes of magnetic fluid V_{MF} values modelled using Equation (5) and related parameters that are summarized in Table 1. The minimum values given in Table 1 are the values of SLP, ς_{MNPs} and Q_{MNPs} for ΔT = 6 °C, which is the minimum requirement to conduct WMS. As can be seen, at the same value of ς_{MNPs}, the SLP required for WMS decreased as the injection volume V_{MF} increased. Similarly, at the same value of SLP, the ς_{MNPs} required for WMS reduced as V_{MF} increased. Furthermore, the maximum temperature increases with the increase in V_{MF} if MNPs have the same SLP and ς_{MNPs} values. The minimum heating power required also reduces when V_{MF} is increased.

With these results, we have estimated a preliminary feasible range for WMS. Although this result is obtained without consideration of blood flow (BF) and cerebrospinal fluid (CSF), it helps us to reduce the ranges of SLP and concentration (ς_{MNPs}) required for investigation (such as for V_{MF} = 0.6 µL, ranges required for investigation: 280 W/g ≤ SLP ≤ 1000 W/g; 28 mg/mL ≤ ς_{MNPs} ≤ 100 mg/mL), thereby significantly reducing the amount of computation required for the brain model.

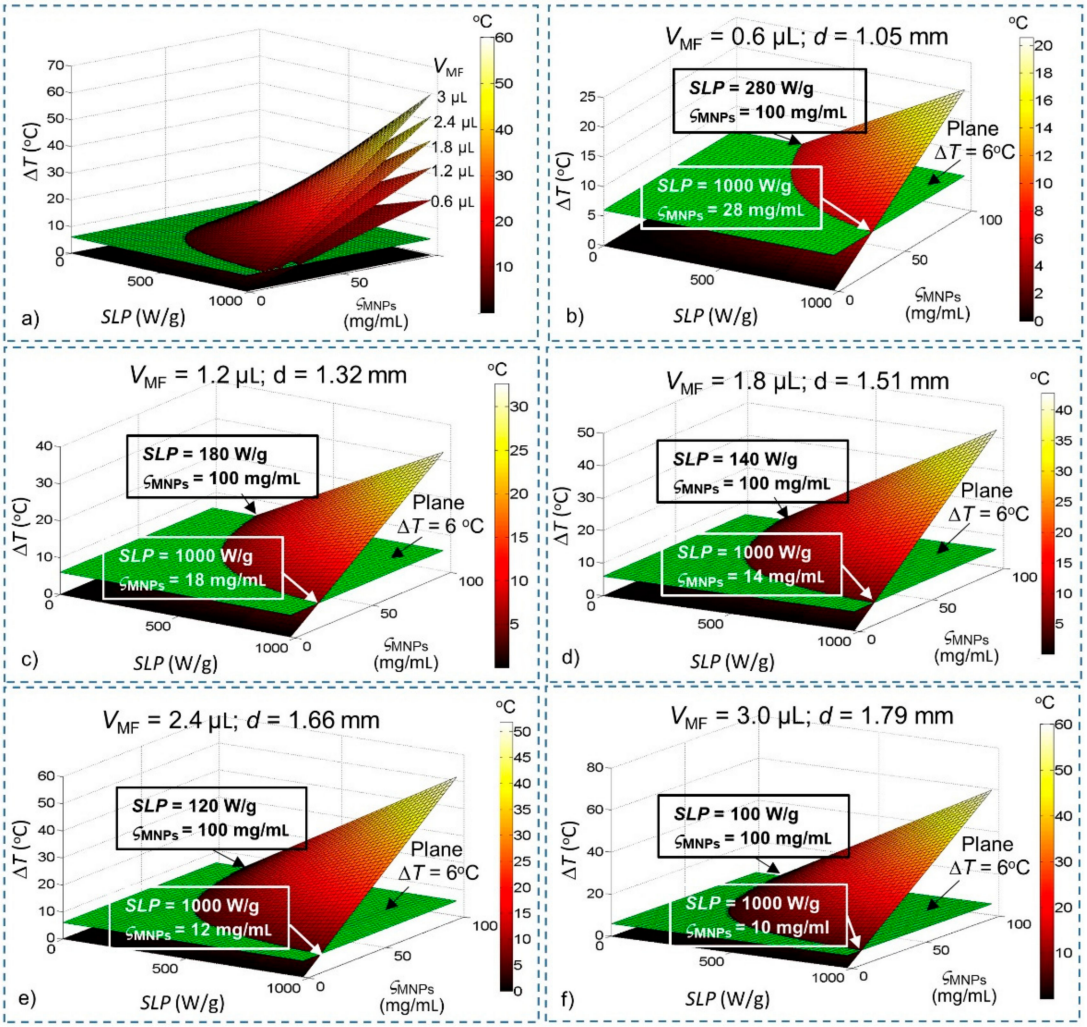

Figure 1. Steady-state temperature change derived from Fourier's law as a function of specific loss power (SLP), concentration (ς_{MNPs}) and volume (V_{MF}) of magnetic nanoparticles (MNPs). Conditions that satisfy the temperature increase $\Delta T > 6$ °C lie above the green plane ($\Delta T = 6$ °C). (**a**) All the different values of V_{MF}; (**b**) $V_{MF} = 0.6$ µL; (**c**) $V_{MF} = 1.2$ µL; (**d**) $V_{MF} = 1.8$ µL; (**e**) $V_{MF} = 2.4$ µL; and (**f**) $V_{MF} = 3.0$ µL.

Table 1. The minimum amount of SLP, ς_{MNPs} and heating power Q_{MNPs} values required for WMS for different values of V_{MF} without considering blood flow (BF) and cerebrospinal fluid (CSF), determined using Fourier's Law.

V_{MF} (µL)	Diameter of Stimulation Region d (mm)	Minimum SLP (W/g) at Maximum ς_{MNPs} (100 mg/mL)	Minimum ς_{MNPs} (mg/mL) at Maximum SLP(1000 W/g)	Maximum ΔT with Maximum SLP and ς_{MNPs} (°C)	Minimum Heating Power Required Q_{MNPs} (W/m^3)
0.6	1.05	280	28	20	2.8×10^7
1.2	1.32	180	18	30	1.8×10^7
1.8	1.51	140	14	40	1.4×10^7
2.4	1.66	120	12	50	1.2×10^7
3.0	1.79	100	10	60	1.0×10^7

2.2. Temperature Distribution inside the Brain before Stimulation

Before finding conditions that satisfy the temperature increase $\Delta T > 6$ °C in the presence of BF and CSF, we need to check the brain model under normal conditions. A simulation without the MNP heating source is developed using the stationary study. The results presented in Figure 2 show that the

temperature of brain tissue is homogeneous at 37 °C, except for a narrow region in the vicinity of its surface near the CSF area. Additionally, the temperature in the brain tissue is higher than the arterial blood temperature due to the 'metabolic temperature shift' T_{m0} = 0.36 °C [20]. The results show that this model adheres to the temperature regulation in the brain. Thus, we can use it in the next step.

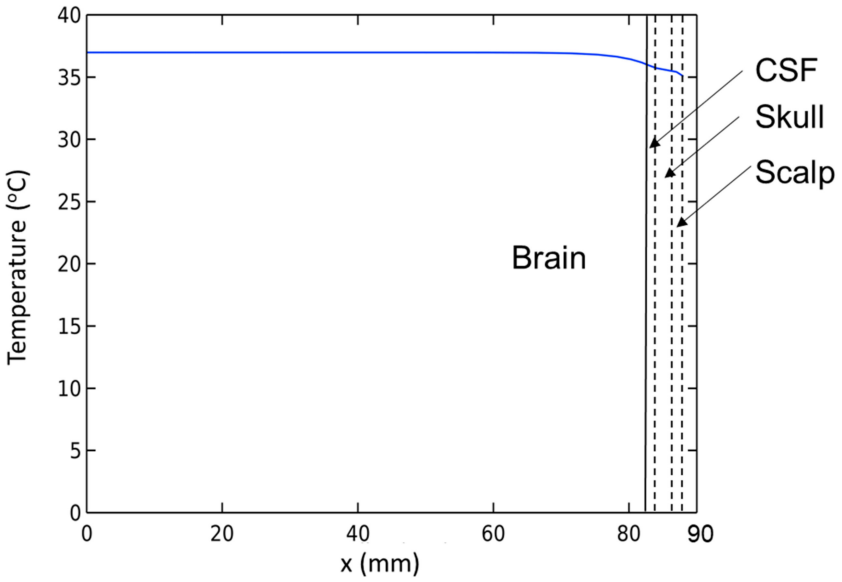

Figure 2. Temperature distribution inside the brain before stimulation.

2.3. Determination of Minimum Limits for WMS in the Presences of Blood Flow and CSF

With the effects of BF and CSF, the steady-state temperatures of MNPs are investigated again to compare them with the results of the simulation without BF and CSF given in Figure 1. The heating source Q_{MNPs} is situated at the center of the brain tissue (for deep brain stimulation). The temperature of MNPs is measured at the center (Figure 3) and at the edge (Figure 4) of the stimulation region. A summary of the results is shown in Table 2 The results show that in the presence of BF and CSF, the required SLP, concentration ς_{MNPs}, and heating power for ΔT = 6 °C increase significantly by about 32%.

Table 2. The minimum amount of SLP, ς_{MNPs} and heating power Q_{MNPs} values required for WMS at different values of V_{MF} with the consideration of BF and CSF from Figures 3 and 4.

V_{MF} (µL)	Minimum SLP (W/g) at Maximum ς_{MNPs} (100 mg/mL)		Minimum ς_{MNPs} (mg/mL) at Maximum SLP (1000 W/g)		Maximum ΔT with Maximum SLP and ς_{MNPs} (°C)		Minimum Heating Power Required Q_{MNPs} (W/m^3)	
	Center	Edge	Center	Edge	Center	Edge	Center	Edge
0.6	370	380	37	38	16.31	15.94	3.7×10^7	3.8×10^7
1.2	240	250	24	25	25.18	24.58	2.4×10^7	2.5×10^7
1.8	190	195	19	19.5	32.36	31.57	1.9×10^7	1.95×10^7
2.4	158	160	15.8	16	38.60	37.65	1.58×10^7	1.6×10^7
3.0	138	140	13.8	14	44.23	43.13	1.38×10^7	1.4×10^7

These results are consistent with the fact that the blood flow plays a significant role in dissipating the heat away from the tissue with the purpose of maintaining the brain temperature at 37 °C. When the hyperthermia process is actually carried out, the blood flow reduces. However, concomitant with the reduction of blood flow, there is a proportional increase in the cerebral metabolic rate [21]. Therefore, assuming that the blood flow rate and the cerebral metabolic rate are constant throughout the WMS process is acceptable [22].

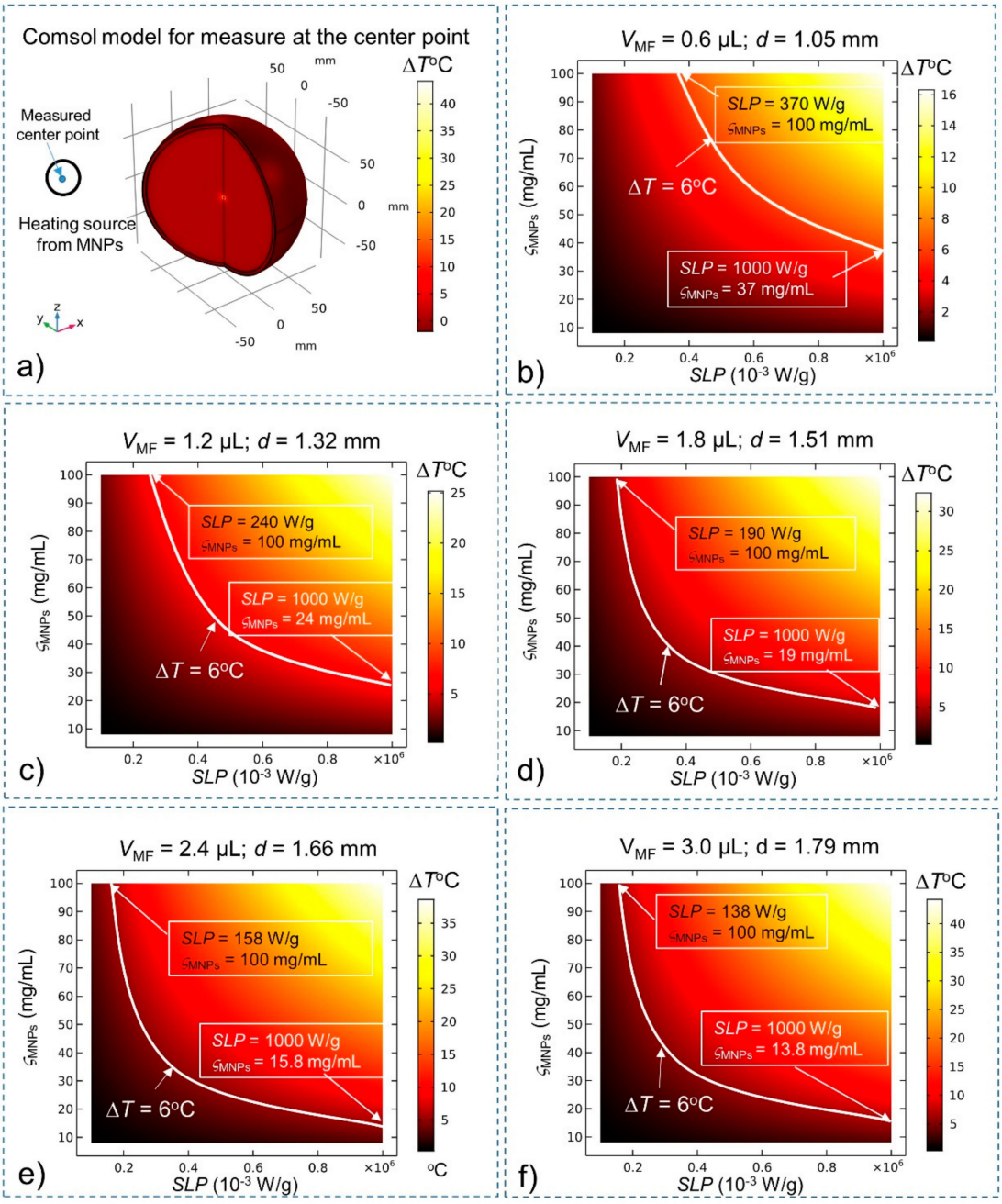

Figure 3. Steady-state temperature at the center of the stimulation region obtained using the bio-heat equation as a function of the SLP, concentration (ς_{MNPs}) and volume (V_{MF}) of MNPs. Conditions that satisfy the temperature increase $\Delta T > 6$ °C lie above the white curve ($\Delta T = 6$ °C). (**a**) Comsol Multiphysics model for measuring temperature at the center of the stimulation region; (**b**) $V_{MF} = 0.6$ µL; (**c**) $V_{MF} = 1.2$ µL; (**d**) $V_{MF} = 1.8$ µL; (**e**) $V_{MF} = 2.4$ µL; and (**f**) $V_{MF} = 3.0$ µL.

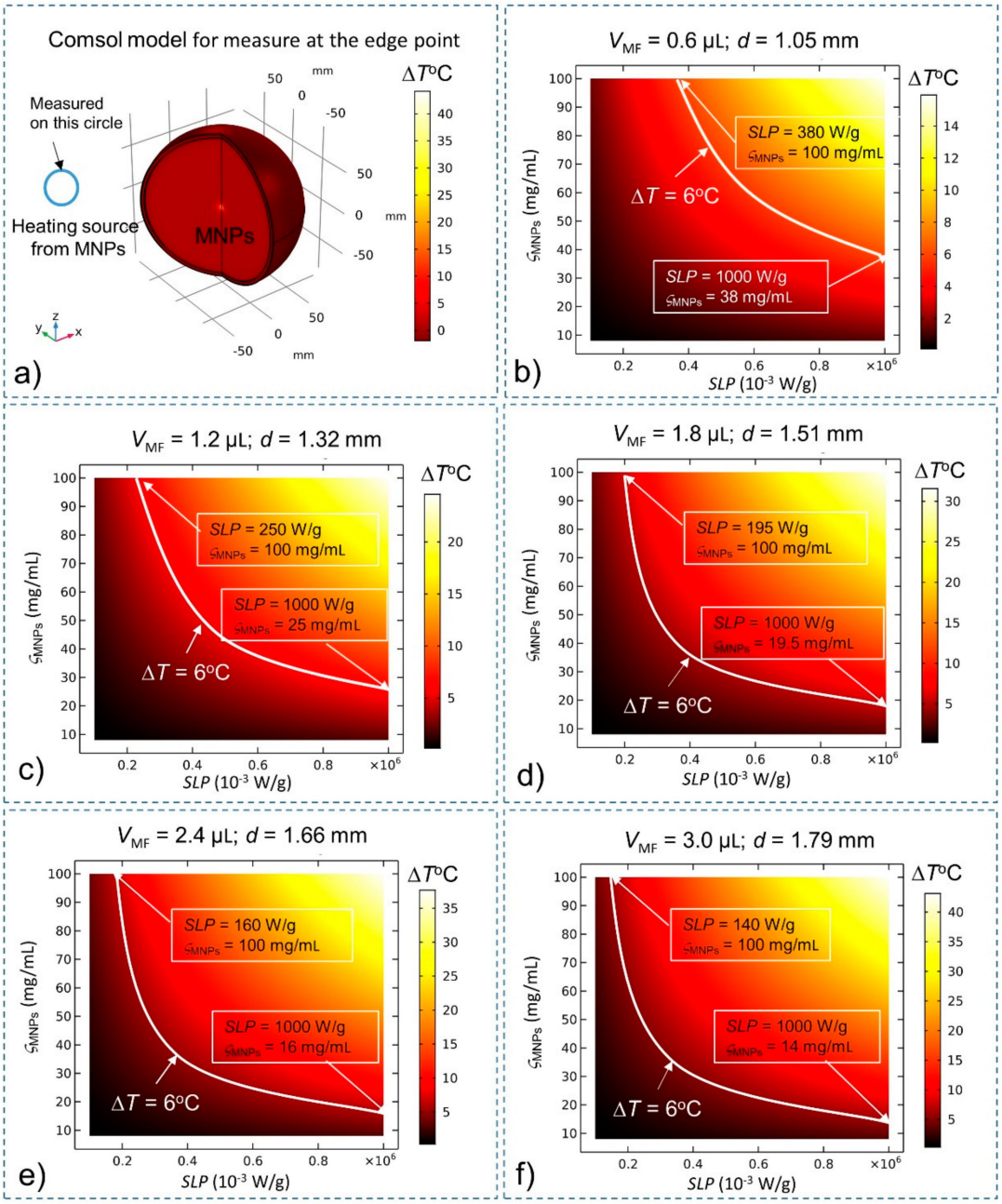

Figure 4. Steady-state temperature at the edge of the stimulation region while considering BF and CSF found using the bio-heat equation as a function of the SLP, concentration (ς_{MNPs}) and volume (V_{MF}) of MNPs. Conditions that satisfy the temperature increase $\Delta T > 6$ °C lie above the white curve (which indicates the increase $\Delta T = 6$ °C) (**a**) Comsol Multiphysics model for measuring temperature at the edge of the stimulation region; (**b**) $V_{MF} = 0.6$ µL; (**c**) $V_{MF} = 1.2$ µL; (**d**) $V_{MF} = 1.8$ µL; (**e**) $V_{MF} = 2.4$ µL; and (**f**) $V_{MF} = 3.0$ µL.

2.4. Prediction of a Feasbile Experiment Condition for WMS

From the results of Equation (14), only minor hyperthermic effects ($P_C < 0.5\%$) are predicted when cells are exposed for 0.5 min to high temperatures of 43–44°C ($S = 0.2$ min^{-1}) as illustrated in Figure 5. A similar result has been concluded in [13].

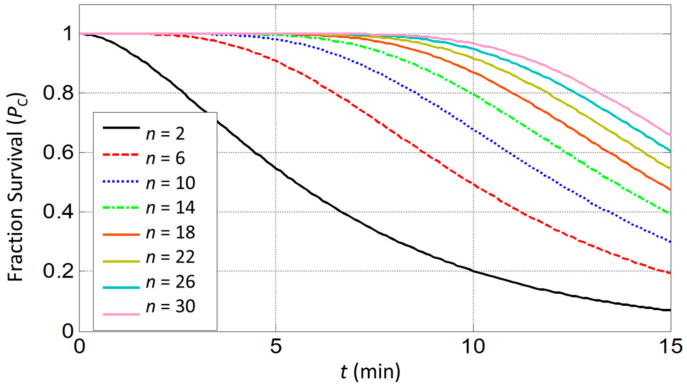

Figure 5. Estimation of cell survival rate in response to prolonged heat exposure at 44 °C for molecular targets n ranging from 2 to 30.

Since the exposure of cells to temperatures from 37–43 °C does not cause serious damage, we only consider the total time (t_{total}) that includes heating time t_1 (from 43 °C to 44 °C) and cooling time t_2 (from 44 °C to 43 °C). The total time t_{total} should be less than 30 s, as shown in Figure 6a.

Firstly, we get a simulation time for the temperature drop from 44 °C to 43 °C in the treatment area as shown in Figure 6b ($T_{initial}$ is equal to 44 °C). We see that the temperature drops below the 43 °C thermal threshold within only 3 s (or $t_2 < 3$ s). In this investigation, we assume that the blood flow rate is constant, so the cooling time depends only on the volume of stimulation (V_{MF}).

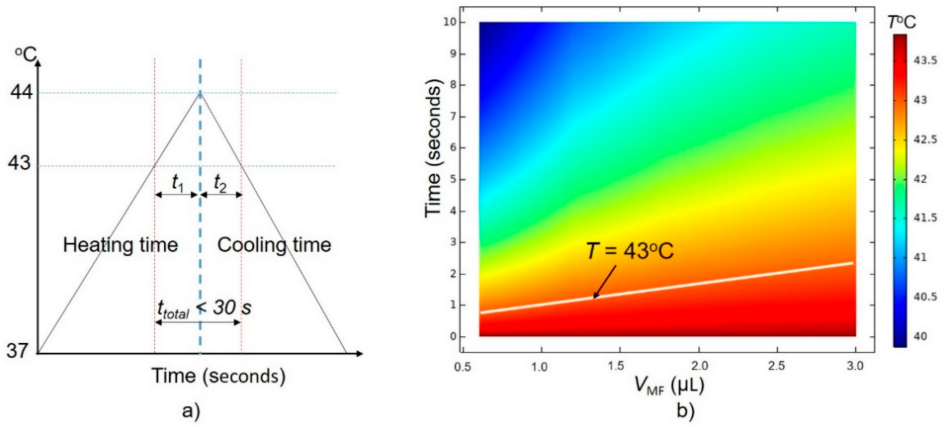

Figure 6. (**a**) A feasible condition for wireless magnetothermal simulation (WMS), (**b**) dependence of cooling time on V_{MF} with the initial temperature of the stimulation treatment equal to 44 °C.

To keep the total time t_{total} below 30 s, the time t_1 should be smaller than 27 s. A time-dependence study is developed with a simulation time of 25 s to find the conditions of SLP and concentration (ς_{MNPs}) that sastify the t_1 condition, with the $T_{initial}$ of the treatment area equal to 43 °C. The final temperature results after 25 s are shown in Figure 7a–e with V_{MF} = 0.6 μL, 1.2 μL, 1.8 μL, 2.4 μL, and 3.0 μL, respectively. A summary of the results shown in Figure 7 is given in Table 3.

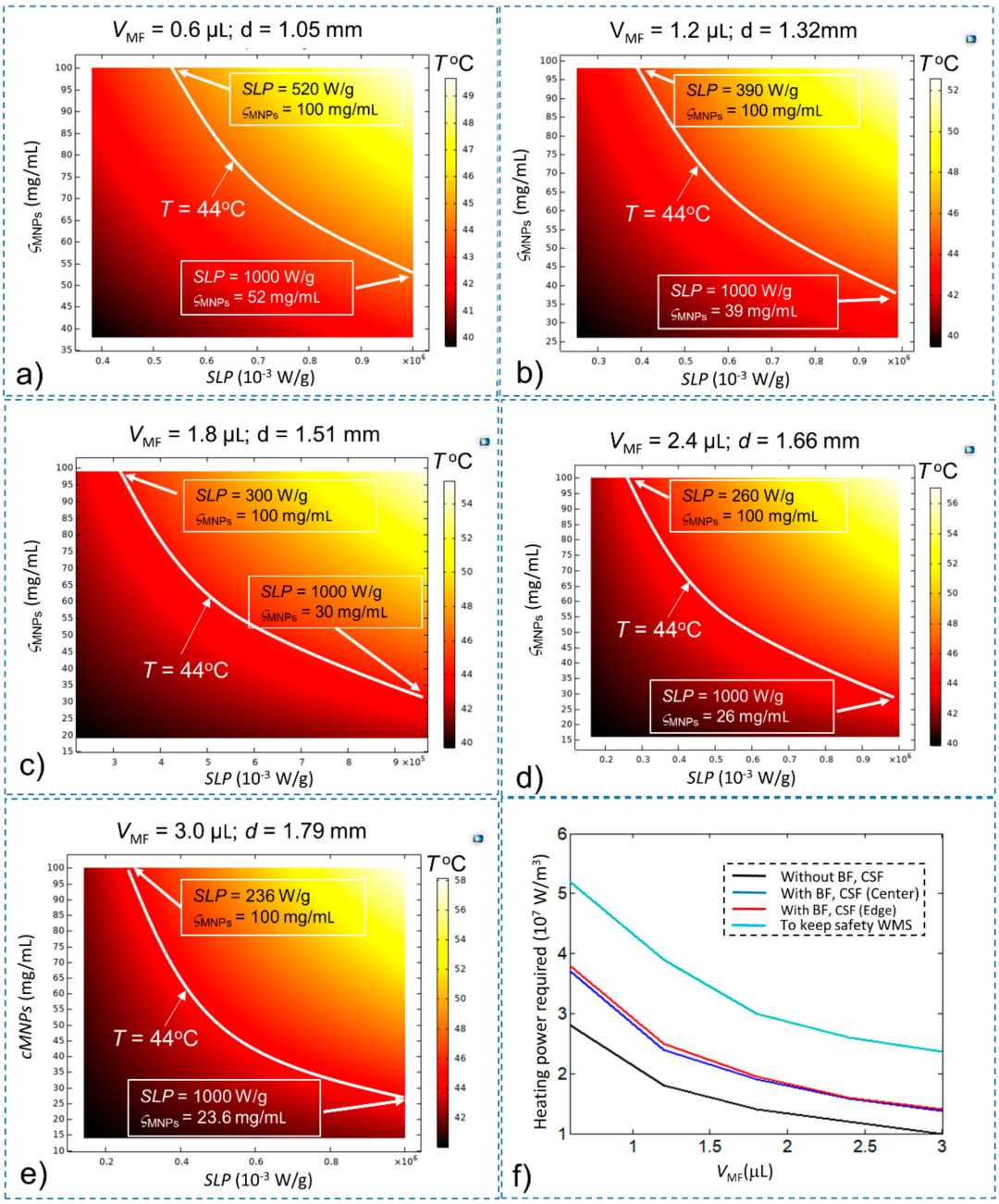

Figure 7. The temperature of the stimulation treatment region after time t = 25 s with $T_{initial}$ = 43 °C for (**a**) V_{MF} = 0.6 µL; (**b**) V_{MF} = 1.2 µL; (**c**) V_{MF} = 1.8 µL; (**d**) V_{MF} = 2.4 µL; (**e**) V_{MF} = 3.0 µL; and (**f**) the minimum heating power Q_{MNPs} required for safe execution of WMS (compared with other conditions).

Table 3. The minimum values of SLP, ς_{MNPs} and heating power Q_{MNPs} values for safe WMS execution with different V_{MF} values.

V_{MF} (µL)	Minimum SLP (W/g) at Maximum ς_{MNPs} (100 mg/mL)	Minimum ς_{MNPs} (mg/mL) at Maximum SLP (1000 W/g)	Minimum Heating Power Required Q_{MNPs} (W/m^3)
0.6	520	52	5.2×10^7
1.2	390	39	3.9×10^7
1.8	300	30	3.0×10^7
2.4	260	26	2.6×10^7
3.0	236	23.6	2.36×10^7

These results show that the required values of SLP, ς_{MNPs} and the heating power to carry out WMS are greater by about 36.8% than those required to satisfy only the temperature increase $\Delta T > 6$ °C. These results were obtained under normal conditions. Depending on the pathology, the parameters for the simulation will need to be recalculated. Appropriate values of SLP, ς_{MNPs} and injection volume (V_{MF}) should be selected depending on the particular application. However, it should be noted that selecting a high SLP is preferable to choosing a high concentration (ς_{MNPs}) as long as the heating power is maintained. This is because with the use of high SLP, we can reduce the injection volume, thus reducing the toxic effect of magnetic particles on the body. In this study, MNPs and SNPs with a core size range of 5–31 nm are considered; magnetite, iron–platinum and maghemite are also suggested for WMS [22] as they can generate high enough heating power, are tolerable by the human body and are immuno-evasive [23]. The commercial MNPs with high stability, homogenous size, high SLP, minimal aggregation and cytotoxicity are also suitable for WMS. However, further development is still required to devise MNPs that have a small size with high SLP to increase their selectivity in targeting the stimulation area and MNPs suitable for both heating and imaging.

In addition, as technologies for measuring particle temperatures in the brain are advancing, monitoring schemes for MNP temperatures such as magnetic particle imaging (MPI) [24] should be incorporated in the WMS process. Moreover, since this simulation assumes that the MNPs are injected directly into the stimulation area, we need to consider how MNPs can reach into the stimulation area. Although a maximum of 7 mg Fe/kg or 510 mg/total dose [25] can be used in humans, to reach an MNP content that satisfies the safety condition is still a challenge. Therefore, the WMS should also be combined with a monitoring magnetic drug delivery system [26,27] and a blood–brain barrier crossing technique [28,29].

3. Materials and Methods

3.1. Fourier's Law for Steady-State Temperature Rise

In the nanoscale world, Rabin showed that conventional heat transfer as defined by Fourier's law is applicable for nanoparticles with sizes larger than 0.3 nm [30]. Thus, Fourier's law is appropriate for the heat distribution analysis in biological tissues during WMS. The steady-state temperature rise at the centre of treated region is given by [30]

$$\Delta T_{MNPs} = \frac{Q_{MNPs} \cdot d^2}{8 \cdot k} \quad (1)$$

where Q_{MNPs} is the heat power density generated by the MNPs or volumeric heating power (W/m^3) [31,32]; k is the thermal conductivity of biological tissues (k = 0.64 W/(m °C) [30]); and d is the diameter of the stimulation region.

The Q_{MNPs} can be determined as shown below [33]:

$$Q_{MNPs} = SLP \cdot \varsigma_{MNPs} \quad (2)$$

where ς_{MNPs} is the concentration of MNPs, which is the ratio of the mass of MNPs and the volume of magnetic fluid (ς_{MNPs} is often given by the manufacturer), and SLP is the specific loss power to determine the amount of electromagnetic energy induced in mass unit of the MNPs. SLP can be represented by the following equation [34]:

$$SLP = \frac{\pi \cdot \mu_0 \cdot \chi''(f) \cdot H^2 \cdot f}{\rho_{MNPs} \cdot \phi} \quad (3)$$

where f and H are the magnetic field frequency and magnetic field strength, respectively, ρ_{MNPs} is the MNP density, ϕ is the MNPs volume fraction, μ_0 is the permeability of free space, and χ'' is the imaginary part of the susceptibility.

SLP can also be explicitly related to measured heating by [35]

$$SLP = \frac{\rho_{water} \cdot C_{water}}{\varsigma_{MNPs}} \cdot \frac{\Delta T}{\Delta t} \quad (4)$$

where T is the measured temperature, t is the time elapsed, C_{water} (4183 J/(kg·K) is the heat capacity of water, and ρ_{water} (998.3 kg/m^3) is the density of water, respectively [35].

To investigate the effects of SLP of MNPs, injection volume of magnetic fluid V_{MF}, and MNPs concentration ς_{MNPs}, Equation (1) is expressed as follows:

$$\Delta T_{MNPs} = \frac{SLP \cdot \varsigma_{MNPs} \cdot \left(6V_{MF}/\pi\right)^{2/3}}{8 \cdot k} \quad (5)$$

where the injection volume of magnetic fluid is equal to $V_{MF} = \pi \cdot d^3/6$.

The magnetic field strength H and magnetic field frequency f affect the temperature rise sigificantly [31]. The commonly used range of magnetic field strength is between 0 and 50 kA/m [35–38]. The commonly used range of frequency is between 100 kHz and 700 kHz [35–38]. However, it is recommended that the product of magnetic field strength and frequency (Hf) should not go beyond 5×10^9 A/(m·s) [38]. To make a system with the abovementioned ranges of magnetic field strength and frequency, we can use an electromagnetic coil with soft ferromagnetic core to enhance the magnetic field and reduce the power requirement of the system [13]. However, this configuration is only advantageous for use with a small workspace, such as for testing a sample or for working at the small animal scale. For larger workspaces, this configuration requires a much larger power system compared to a solenoid coil [39,40]. A solenoid coil system, such as a heat induction system [19], is proposed for larger workspaces. However, creating a human scaled system is still a big challenge as it is required to have a huge capacity, which makes the system very expensive and raises safety issues.

In this safety condition ($H \cdot f \leq 5 \times 10^9$ A/(m·s)), the SLP and ς_{MNPs} values for various commercial MNPs such as SHA-25 from Ocean Nanotech [38], BNF-Dextran from Micromod [36], JHU from Nano Materials Technology [36], HyperMag from NanoTherics [35] and other types of MNPs [37] are summarized in Table 4. While operating within the safety conditions, magnetic field strength and frequency values can be represented by the SLP values, and their relationship is shown in Equation (3). In addition, Q_{MNPs} depends on the SLP as shown in Equation (2). Thus, to simplify the analysis, we have used the SLP values instead of using both the magnetic field strength and frequency values to change Q_{MNPs}. Utilizing values of the SLP without creating a simulation model for the magnetic field can greatly simplify the simulation computation when it is applied to the brain model.

Table 4. Safe ranges of SLP, injection volume (V_{MF}) and concentration (ς_{MNPs}) values for investigation.

Name	Minimal Value	Maximal Value
SLP (W/g)	0	1000
ς_{MNPs} (mg/mL)	0	100
V_{MF} (μL)	0	3

The type of particles used in this study are MNPs or SNPs with a core size range of 5–31 nm. For particles with a size at the micro or nano-scale, the dominant source of heating is hysteresis loss [32]. In the case of SNPs, these nano-sized particles exhibit a narrow hysteresis, and the major contributor to temperature rise is heating via Néelian and Brownian relaxation [41,42].

Rabin et al. proposed that a minimal region with a diameter d of 0.9 mm (or an equivalent volume V_{MF} = 0.38 μL) occupied by nanoparticles was required to increase the temperature at the center of a tissue by 6 °C for hyperthermia with an average heating power of about 4×10^7 W/m^3 [30]. A minimum volume of MNPs is necessary to minimize their toxic effect. However, the stimulation volume can be changed depending on the area of stimulation and the type of disease. So, in this paper, we investigate

the range of volume up to 3 μL, as shown in Table 1. Equation (5) does not consider the effects of blood flow (BF) and cerebrospinal fluid (CSF) as part of the main limitations. However, it is much simpler to use than the bio-heat equation described in Section 3.2. Therefore, Equation (5) is used to estimate the minimum value required for stimulation and to minimize the range of SLP, concentration ς_{MNPs}, and stimulation volume V_{MF} required for investigation when considering the brain model.

3.2. Bio-Heat Transfer Model for Heat Distribution

During stimulation, unlike hyperthermia, the temperature of neural cells should be increased and then brought back to 37 °C quickly to avoid causing any thermal damage [43]. Therefore, the transient heat evolution of the infused MNPs need to be considered.

In the presence of BF and CSF, the increase of temperature is non-linear due to heat loss, and its rise rate reduces until it reaches the steady state. Therefore, the bioheat transfer model is established to describe the heat transfer in biological tissues. This model can be used to determine operation time for stimulation and cooling while taking into account the heat loss due to BF and CSF.

Although the real geometry of the human brain is complicated, we can use the simple geometry shown in Figure 8 because the temperature in the brain is (a) practically homogeneous except for a narrow region Δ in the vicinity of its surface (with only several millimeters of Δ, it is much smaller than an adult human brain size of 15 cm) and (b) practically independent of specific brain geometry [20]. The brain is modeled as a sphere of brain tissue with overlaying layers of CSF, skull and scalp. The outermost layer represents the scalp, the next layer represents the skull, the third layer represents the CSF, and the solid sphere at the center represents the brain. The model is shown in more detail in Figure 8.

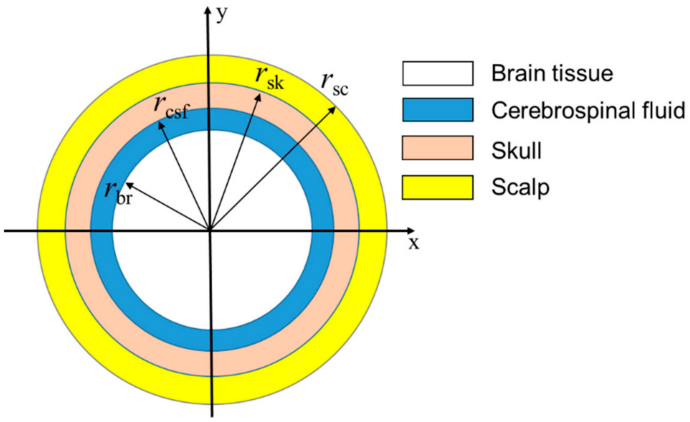

Figure 8. Simplified human brain model.

The bioheat transfer equations for the brain model can be expressed as follows [22,32,35,44]:

$$\rho_{br}C_{br}\frac{\partial T_{br}}{\partial t} = k_{br}\nabla^2 T_{br} + \rho_b C_b \omega_{br}(T_b - T_{br}) + Q_{m\_br} + Q_{MNPs} \quad (6)$$

$$\rho_{csf}C_{csf}\frac{\partial T_{csf}}{\partial t} = k_{csf}\nabla^2 T_{csf} \quad (7)$$

$$\rho_{sk}C_{sk}\frac{\partial T_{sk}}{\partial t} = k_{sk}\nabla^2 T_{sk} \quad (8)$$

$$\rho_{sc}C_{sc}\frac{\partial T_{sc}}{\partial t} = k_{sc}\nabla^2 T_{sc} \quad (9)$$

where ρ_{br}, ρ_{csf}, ρ_{sk}, and ρ_{sc} are the densities of the brain, CSF, skull and scalp, respectively. C_{br}, C_{csf}, C_{sk}, and C_{sc} are the specific heat of the brain, CSF, skull and scalp, respectively. k_{br}, k_{csf}, k_{sk}, and k_{sc} are the thermal conductivity of the brain, CSF, skull and scalp, respectively. T_{br}, T_{csf}, T_{sk}, T_{sc}, T_b and

T_{env} are the temperature of the brain, CSF, skull, scalp, arterial blood, and the surroundings of the brain, respectively. Q_{m_br} is the internal heat generation of the brain tissue due to cerebral metabolism. Q_{MNPs} is obtained using Equation (2).

The brain temperature is expected to be higher than that of the arterial blood due to the 'metabolic temperature shift' (T_{m0} = 0.36 °C) [20]. While the arterial blood temperature T_b = 36.64 °C, the initial temperature of the brain composition T_0 is 37 °C. The physical parameters of the brain composition used in the brain model are given in Table 5.

In CSF, blood flow rate and metabolic heat production are absent. In the scalp and skull, these quantities are very small [45] and so can be ignored. Therefore, the temperature distribution in CSF, skull, and scalp can be described by the simplified Equations (7)–(9). We only consider the blood flow rate and metabolic rate in the brain tissue, as given in Equation (6).

Table 5. Physical parameters used in the simulation [13,20,46,47].

Parameters	Specific Heat C (J/(kg °C))	Density ρ (kg/m^3)	Thermal Conductivity k (W/(m °C))	Blood Flow Rate ω (1/s)	Metabolic Rate Q_m (W/m^3)	Radius (Adult) r (mm)	Temperature T_b (°C)	Initial Temperature T_0 (°C)
Blood (b)	3800	1050	0.5	–	–	–	36.64	36.64
Scalp (sc)	4000	1000	0.34	0.00143	363	88	37.00	37.00
Skull (sk)	2300	1500	1.16	0.000143	70	87	37.00	37.00
CSF	3800	1007	0.61	0	0	84	37.00	37.00
Brain tissue (br)	3700	1050	0.51	0.008	10437	83	37.00	37.00
Brain surroundings	–	–	–	–	–	–	25.00	25.00

– is no value.

Heat exchange with air can modify the uniformity of the brain temperature distribution near the brain surface. To address this issue, Equations (6)–(9) need to be solved along with the boundary conditions at the interfaces; i.e., the brain/CSF, CSF/skull, skull/scalp, and scalp/air interfaces. These boundary conditions reflect the fact that no heat dissipation takes place on the interfaces between the regions; hence, temperature and the normal component of heat flow should be continuous at each of these interfaces. The heat exchange between the scalp and air at a given temperature T_{env} is described by the heat transfer coefficient, h = 12 W/(m^{2}K). Thus, we have the following boundary equations:

$$T_{0\_br}(r_{br}) = T_{0\_csf}(r_{br}),\ k_{br}\frac{\partial T_{br}}{\partial t} = k_{csf}\frac{\partial T_{csf}}{\partial t} \tag{10}$$

$$T_{0\_csf}(r_{csf}) = T_{0\_sk}(r_{csf}),\ k_{csf}\frac{\partial T_{csf}}{\partial t} = k_{sk}\frac{\partial T_{sk}}{\partial t} \tag{11}$$

$$T_{0\_sk}(r_{sk}) = T_{0\_sc}(r_{sk}),\ k_{sk}\frac{\partial T_{sk}}{\partial t} = k_{sc}\frac{\partial T_{sc}}{\partial t} \tag{12}$$

$$k_{sc}\nabla T_{sc} = h(T_{sc} - T_{env}) \tag{13}$$

This model is developed using COMSOL Multiphysics software (Version 5.4) with bioheat transfer physics, stationary and time dependence Studies.

3.3. Cytotoxic Effects

To find a feasible condition for WMS, the probability P_C of a cell surviving an exposure for time t (min) to a temperature is considered using the given equation [43]:

$$P_C = 1 - \left(1 - (1 - S)^t\right)^n \tag{14}$$

where S is the inactivation rate of a molecular target of number n. The S-parameter varies from 0.015 to 0.2 min^{-1} in the temperature range 43–44 °C [48]. A target representing a single protein, DNA, or membrane, is inconsistent with this model. Almost all proteins present more than a few copies per

cell, which is implied by the small values of n observed. The target number n is assumed to vary from 2–30 based on prior model fitting to empirical results [30]. The rate of death is highly dependent on the thermal history of the cells. Thus, the determination of the exact inactivation rate for a general condition is very complicated. Therefore, to predict a feasible condition for WMS before performing experiments, the inactivation rate is selected as the maximum value or $S = 0.2\ \text{min}^{-1}$.

4. Conclusions

Stimulation of the deep brain has shown outstanding performance for people with neurological problems. Although there are several more invasive stimulation methods, WMS has emerged as a promising, less invasive alternative with numerous advantages such as being fast, tetherless, and implanted device-free. To ensure the safe operation of WMS, the magnetic strength and frequency are limited ($H{\cdot}f \leq 5 \times 10^9$ A/(m·s). With the current technology, only the selction of a range of SLP and ς_{MNPs} is possible, which we have done based on previous studies. Then, we presented a simulation scheme for WMS using steady-state temperature equations based on Fourier's law to determine a preliminary requirement for SLP, concentration, MNP volume and heating power. A simple brain model satisfying the temperature regulation in the brain was developed using the bioheat transfer equation in Comsol Multiphysics$^{\text{TM}}$ software. In the presence of BF and CSF, the requirements for SLP, concentration, MNPs volume and heating power needed were found to be higher than those found using the equations based on Fourier's law. In addition, a feasible condition for WMS was suggested based on the cytotoxic effects and the simulation results. A preliminary review of the simulation results shows that the heating power required to carry out WMS is greater by about 36.8% than that required to satisfy only the temperature increase $\Delta T = 6\ ^\circ\text{C}$. This result will be quite helpful for researchers in selecting adequate MNPs to use for WMS. Our future work will include practical experiments in a mouse brain, as well as the development of a brain model that can depict real circumstances.

Author Contributions: T.-A.L. and J.Y. conceived the idea and designed the study for the modeling method, analyzed the data, and wrote the paper. M.P.B. helped with the simulation and drew the figures. All authors have read and approved the manuscript.

Funding: This research was funded by the National Research Foundation (NRF) of Korea (2017R1A2B4011704 & 2019M3C1B8090798) and Korea Evaluation Institute of Industrial Technology (KEIT) grant funded by the Korea government (MOTIE) (No. 20003822, Development of Navigation System Technologies of Micro-Nano Robots with Drug for Brain Disease Therapy).

Acknowledgments: The authors acknowledge the help provided by Amre Eizad in the writing of this paper.

Conflicts of Interest: The authors declare no conflict of interest.

Abbreviations

SLP	Specific loss power
SNPs	Super paramagnetic nanoparticles
MNPs	Magnetic nanoparticles
WMS	Wireless magnetothermal stimulation
CSF	Cerebrospinal fluid
BF	Blood flow
MF	Magnetic fluid
AMF	Alternating magnetic fields

References

1. Wyszkowska, J.; Jankowska, M.; Gas, P. Electromagnetic fields and neurodegenerative diseases. *Przegląd Elektrotechniczny* **2019**, *95*, 229–257. [CrossRef]
2. Perlmutter, J.S.; Mink, J.W. Deep brain stimulation. *Annu. Rev. Neurosci.* **2006**, *29*, 229–257. [CrossRef]
3. Banghart, M.; Borges, K.; Isacoff, E.; Trauner, D.; Kramer, R.H. Light-activated ion channels for remote control of neuronal firing. *Nat. Neurosci.* **2004**, *7*, 1381–1386. [CrossRef]

4. Tufail, Y.; Matyushov, A.; Baldwin, N.; Tauchmann, M.L.; Georges, J.; Yoshihiro, A.; Tillery, S.I.H.; Tyler, W.J. Transcranial pulsed ultrasound stimulates intact brain circuits. *Neuron* **2010**, *66*, 681–694. [CrossRef]
5. Walsh, V.; Cowey, A. Transcranial magnetic stimulation and cognitive neuroscience. *Nat. Rev. Neurosci.* **2000**, *1*, 73. [CrossRef]
6. Boyden, E.S.; Zhang, F.; Bamberg, E.; Nagel, G.; Deisseroth, K. Millisecond-timescale, genetically targeted optical control of neural activity. *Nat. Neurosci.* **2005**, *8*, 1263. [CrossRef]
7. Wu, W.; Wu, Z.; Yu, T.; Jiang, C.; Kim, W.-S. Recent progress on magnetic iron oxide nanoparticles: Synthesis, surface functional strategies and biomedical applications. *Sci. Technol. Adv. Mater.* **2015**, *16*, 23501. [CrossRef]
8. Kurgan, E.; Gas, P. Magnetophoretic placement of ferromagnetic nanoparticles in rf hyperthermia. In Proceedings of the 2017 Progress in Applied Electrical Engineering (PAEE), Koscielisko, Poland, 25–30 June 2017; pp. 1–4.
9. Périgo, E.A.; Hemery, G.; Sandre, O.; Ortega, D.; Garaio, E.; Plazaola, F.; Teran, F.J. Fundamentals and advances in magnetic hyperthermia. *Appl. Phys. Rev.* **2015**, *2*, 041302. [CrossRef]
10. Wiley, D.T.; Webster, P.; Gale, A.; Davis, M.E. Transcytosis and brain uptake of transferrin-containing nanoparticles by tuning avidity to transferrin receptor. *Proc. Natl. Acad. Sci. USA* **2013**, *110*, 8662–8667. [CrossRef]
11. Pankhurst, Q.A.; Connolly, J.; Jones, S.K.; Dobson, J. Applications of magnetic nanoparticles in biomedicine. *J. Phys. D: Appl. Phys.* **2003**, *36*, 167–181. [CrossRef]
12. Maysinger, D.; Ji, J.; Hutter, E.; Cooper, E. Nanoparticle-based and bioengineered probes and sensors to detect physiological and pathological biomarkers in neural cells. *Front. Neurosci.* **2015**, *9*, 480. [CrossRef] [PubMed]
13. Chen, R.; Romero, G.; Christiansen, M.G.; Mohr, A.; Anikeeva, P. Wireless magnetothermal deep brain stimulation. *Science* **2015**, *347*, 1477–1480. [CrossRef] [PubMed]
14. Syrek, P.; Skowron, M.; Ciesla, A. Passive shielding of magnetic field in transcranial magnetic stimulation–outline of the problem. In Proceedings of the 2019 11th International Symposium on Advanced Topics in Electrical Engineering (ATEE), Bucharest, Romania, Romania, 28–30 March 2019; pp. 1–4.
15. Caterina, M.J.; Schumacher, M.A.; Tominaga, M.; Rosen, T.A.; Levine, J.D.; Julius, D. The capsaicin receptor: A heat-activated ion channel in the pain pathway. *Nature* **1997**, *389*, 816. [CrossRef] [PubMed]
16. Tominaga, M.; Caterina, M.J.; Malmberg, A.B.; Rosen, T.A.; Gilbert, H.; Skinner, K.; Raumann, B.E.; Basbaum, A.I.; Julius, D. The cloned capsaicin receptor integrates multiple pain-producing stimuli. *Neuron* **1998**, *21*, 531–543. [CrossRef]
17. Huang, H.; Delikanli, S.; Zeng, H.; Ferkey, D.M.; Pralle, A. Remote control of ion channels and neurons through magnetic-field heating of nanoparticles. *Nat. Nanotechnol.* **2010**, *5*, 602. [CrossRef] [PubMed]
18. Stanley, S.A.; Gagner, J.E.; Damanpour, S.; Yoshida, M.; Dordick, J.S.; Friedman, J.M. Radio-wave heating of iron oxide nanoparticles can regulate plasma glucose in mice. *Science* **2012**, *336*, 604–608. [CrossRef] [PubMed]
19. Munshi, R.; Qadri, S.M.; Zhang, Q.; Rubio, I.C.; del Pino, P.; Pralle, A. Magnetothermal genetic deep brain stimulation of motor behaviors in awake, freely moving mice. *eLife* **2017**, *6*, e27069. [CrossRef] [PubMed]
20. Sukstanskii, A.L.; Yablonskiy, D.A. Theoretical model of temperature regulation in the brain during changes in functional activity. *Proc. Natl. Acad. Sci. USA* **2006**, *103*, 12144–12149. [CrossRef]
21. Nybo, L.; Møller, K.; Volianitis, S.; Nielsen, B.; Secher, N.H. Effects of hyperthermia on cerebral blood flow and metabolism during prolonged exercise in humans. *J. Appl. Physiol.* **2002**, *93*, 58–64. [CrossRef]
22. Patterson, J.; Strang, R. The role of blood flow in hyperthermia. *Int. J. Radiat. Oncol. Biol. Phys.* **1979**, *5*, 235–241. [CrossRef]
23. Hergt, R.; Hiergeist, R.; Hilger, I.; Kaiser, W.A.; Lapatnikov, Y.; Margel, S.; Richter, U. Maghemite nanoparticles with very high ac-losses for application in rf-magnetic hyperthermia. *J. Magn. Magn. Mater.* **2004**, *270*, 345–357. [CrossRef]
24. Zhong, J.; Schilling, M.; Ludwig, F. Spatial and temperature resolutions of magnetic nanoparticle temperature imaging with a scanning magnetic particle spectrometer. *Nanomaterials* **2018**, *8*, 866. [CrossRef]
25. Mason, E.E.; Cooley, C.Z.; Cauley, S.F.; Griswold, M.A.; Conolly, S.M.; Wald, L.L. Design analysis of an mpi human functional brain scanner. *Int. J. Magn. Part. Imaging* **2017**, *3*, 1703008.
26. Le, T.-A.; Zhang, X.; Hoshiar, A.K.; Yoon, J. Real-time two-dimensional magnetic particle imaging for electromagnetic navigation in targeted drug delivery. *Sensors* **2017**, *17*, 2050. [CrossRef]

27. Zhang, X.; Le, T.-A.; Hoshiar, A.K.; Yoon, J. A soft magnetic core can enhance navigation performance of magnetic nanoparticles in targeted drug delivery. *IEEE/ASME Trans. Mechatron.* **2018**, *23*, 1573–1584. [CrossRef]
28. Hoshiar, A.; Le, T.-A.; Amin, F.; Kim, M.; Yoon, J. A novel magnetic actuation scheme to disaggregate nanoparticles and enhance passage across the blood–brain barrier. *Nanomaterials* **2017**, *8*, 3. [CrossRef]
29. Amin, F.U.; Hoshiar, A.K.; Do, T.D.; Noh, Y.; Shah, S.A.; Khan, M.S.; Yoon, J.; Kim, M.O. Osmotin-loaded magnetic nanoparticles with electromagnetic guidance for the treatment of alzheimer's disease. *Nanoscale* **2017**, *9*, 10619–10632. [CrossRef]
30. Rabin, Y. Is intracellular hyperthermia superior to extracellular hyperthermia in the thermal sense? *Int. J. Hyperth.* **2002**, *18*, 194–202. [CrossRef]
31. Jordan, A.; Scholz, R.; Wust, P.; Schirra, H.; Schiestel, T.; Schmidt, H.; Felix, R. Endocytosis of dextran and silan-coated magnetite nanoparticles and the effect of intracellular hyperthermia on human mammary carcinoma cells in vitro. *J. Magn. Magn. Mater.* **1999**, *194*, 185–196. [CrossRef]
32. Ng, E.Y.K.; Kumar, S.D. Physical mechanism and modeling of heat generation and transfer in magnetic fluid hyperthermia through néelian and brownian relaxation: A review. *Biomed. Eng. Online* **2017**, *16*, 36.
33. Kozissnik, B.; Bohorquez, A.C.; Dobson, J.; Rinaldi, C. Magnetic fluid hyperthermia: Advances, challenges, and opportunity. *Int. J. Hyperth.* **2013**, *29*, 706–714. [CrossRef] [PubMed]
34. Noh, S.-H.; Moon, S.H.; Shin, T.-H.; Lim, Y.; Cheon, J. Recent advances of magneto-thermal capabilities of nanoparticles: From design principles to biomedical applications. *Nano Today* **2017**, *13*, 61–76. [CrossRef]
35. Gas, P.; Miaskowski, A. Specifying the ferrofluid parameters important from the viewpoint of magnetic fluid hyperthermia. In Proceedings of the 2015 Selected Problems of Electrical Engineering and Electronics (WZEE), Kielce, Poland, 17–19 September 2015; pp. 1–6.
36. Soetaert, F.; Kandala, S.K.; Bakuzis, A.; Ivkov, R. Experimental estimation and analysis of variance of the measured loss power of magnetic nanoparticles. *Sci. Rep.* **2017**, *7*, 6661. [CrossRef] [PubMed]
37. Hervault, A.; Thanh, N.T.K. Magnetic nanoparticle-based therapeutic agents for thermo-chemotherapy treatment of cancer. *Nanoscale* **2014**, *6*, 11553–11573. [CrossRef] [PubMed]
38. Schuerle, S.; Dudani, J.S.; Christiansen, M.G.; Anikeeva, P.; Bhatia, S.N. Magnetically actuated protease sensors for in vivo tumor profiling. *Nano Lett.* **2016**, *16*, 6303–6310. [CrossRef]
39. Christiansen, M.G. Magnetothermal multiplexing for biomedical applications. Massachusetts Institute of Technology. Ph.D. Thesis, Massachusetts Institute of Technology, Cambridge, MA, USA, 2017.
40. Gas, P.; Kurgan, E. Cooling effects inside water-cooled inductors for magnetic fluid hyperthermia. In Proceedings of the 2017 Progress in Applied Electrical Engineering (PAEE), Koscielisko, Poland, 25–30 June 2017; pp. 1–4.
41. Okawa, K.; Sekine, M.; Maeda, M.; Tada, M.; Abe, M.; Matsushita, N.; Nishio, K.; Handa, H. Heating ability of magnetite nanobeads with various sizes for magnetic hyperthermia at 120 khz, a noninvasive frequency. *J. Appl. Phys.* **2006**, *99*, 08H102. [CrossRef]
42. Dutz, S.; Hergt, R. Magnetic nanoparticle heating and heat transfer on a microscale: Basic principles, realities and physical limitations of hyperthermia for tumour therapy. *Int. J. Hyperth.* **2013**, *29*, 790–800. [CrossRef]
43. Lepock, J.R. Cellular effects of hyperthermia: Relevance to the minimum dose for thermal damage. *Int. J. Hyperth.* **2003**, *19*, 252–266. [CrossRef]
44. Diller, K.R. Fundamentals of bioheat transfer. *Phys. Therm. Ther. Fundam. Clin. Appl.* **2012**, 3–22.
45. Olsen, R.; Hayes, L.; Wissler, E.; Nikaidoh, H.; Eberhart, R. Influence of hypothermia and circulatory arrest on cerebral temperature distributions. *J. Biomech. Eng.* **1985**, *107*, 354–360. [CrossRef]
46. Diao, C.; Zhu, L.; Wang, H. Cooling and rewarming for brain ischemia or injury: Theoretical analysis. *Ann. Biomed. Eng.* **2003**, *31*, 346–353. [CrossRef] [PubMed]
47. Sukstanskii, A.; Yablonskiy, D. Theoretical limits on brain cooling by external head cooling devices. *Eur. J. Appl. Physiol.* **2007**, *101*, 41–49. [CrossRef] [PubMed]
48. Leith, J.T.; Miller, R.C.; Gerner, E.W.; Boone, M.L. Hyperthermic potentiation. Biological aspects and applications to radiation therapy. *Cancer* **1977**, *39*, 766–779. [CrossRef]